International Journal of Computational Methods and Experimental Measurements
https://www.acadlore.com/journals/IJCMEM

# Experimental Testing of Earth to Air Heat Exchanger for Air Conditioning of Greenhouse in Hot Climate Regions

Hussein L. Thamer*, Mushtaq I. Hasan

Department of Mechanical Engineering, College of Engineering, University of Thi-Qar, 64001 Thi-Qar, Iraq

* Correspondence: Hussein L. Thamer (hussein.l.t@utq.edu.iq)

**Received:** 10-28-2025 **Revised:** 12-12-2025 **Accepted:** 12-24-2025

**Citation:** H. L. Thamer and M. I. Hasan, "Experimental testing of earth to air heat exchanger for air conditioning of greenhouse in hot climate regions," *Int. J. Comput. Methods Exp. Meas.*, vol. 13, no. 4, pp. 908–927, 2025. https://doi.org/10.56578/ijcmem130412.



**Abstract:** Increasing energy requirements in hot regions highlight the need for sustainable thermal management technologies. A promising passive cooling solution is Earth-Air Heat Exchanger (EAHE) that use the relatively stable temperature of the subsurface soil to pre-cool air supplied to indoor spaces. This study investigates the thermal and hydraulic performance of an EAHE coupled to a greenhouse in severe summer conditions in Nasiriyah city, southern Iraq, experimentally. The system was designed to evaluate its effectiveness in moderating ambient temperature extremes and reducing mechanical cooling energy requirements. Experimental results during July–October showed that the EAHE outlet air temperature stayed between 31 and 38°C despite ambient temperature exceeding 50°C, indicating a stable thermal response of the buried exchanger. The greenhouse air temperature was maintained at 34–40°C during peak daytime hours and decreased to about 29–33°C during the remaining operating periods, confirming improved internal thermal conditions. The thermal effectiveness ($\varepsilon$) ranged from 0.68 to 0.75, and the average temperature drop ($\Delta T$) was above 13°C throughout the test period. Furthermore, pressure drop and fan power increased with airflow velocity, consistent with a turbulent flow regime. The EAHE delivered 2011–2942 W of cooling with 42–144 W of fan power; an indicative baseline from a comparable 50 Hz mini-split (8500–11000 Btu/h) shows a rated electrical input of 880–1070 W, highlighting the low electrical demand of the EAHE fan (catalog-based context, not a side-by-side test). In summary, the EAHE–greenhouse system demonstrates a viable, energy-efficient pilot-scale option for passive cooling in hot climates, with potential for agricultural applications subject to site-specific sizing and installation constraints.

**Keywords:** Passive cooling systems; Earth-Air Heat Exchanger; Greenhouse cooling; Hot climate regions; Thermal–hydraulic performance

## 1 Introduction

Due to the increasing demand for energy in hot regions and the requirement for sustainable cooling technologies, Earth-Air Heat Exchanger (EAHE) systems represent a viable passive approach for saving energy on air-conditioning systems, mainly in greenhouses. These systems take advantage of the relatively constant temperature at 3–4 meters depth to pre-condition incoming air before delivery into spaces. Through this approach, the dependency on active air-conditioning systems can be reduced substantially, which can improve indoor thermal comfort. The utilization of thermal techniques in agriculture and other sectors has increased in parallel with the global trend toward adopting energy-efficient and sustainable technologies for thermal management.

Analyzing the performance of the Earth-to-Air Heat Exchanger is challenging due to the numerous related aspects that require in-depth investigation, such as the heat transfer rate, overall thermal efficiency, pressure losses, long-term operating reliability, and economic feasibility. As the demand for EAHE systems increases, many studies have been conducted to evaluate their performance under various climatic conditions, configurations, and operational scenarios.

Across the EAHE literature, performance is consistently governed by a small set of coupled design and operating factors: (i) airflow rate/velocity, (ii) pipe geometry and layout (diameter, length, and pipe arrangement), and (iii) soil thermal conditions and properties. These factors jointly determine a key engineering trade-off: higher airflow can increase delivered cooling capacity but usually at the cost of higher-pressure losses and fan energy, while longer/deeper or better-coupled pipes improve thermal exchange with diminishing returns.

From the hydraulic point of view, there are many investigations that have shown that the geometry highly affects the pressure-loss features. Amanowicz and Wojtkowiak [1] conducted a study on the non-uniformity of air flow in EAHE U- and Z-type multi-pipe EAHE systems in which they found that simple geometry modifications could allow for nearly 9% improvement in both flow uniformity and heat transfer without any additional costs. They also showed in a series of subsequent works [2, 3] that manifold design and configuration could lead to large differences between airflow allocations-varying up to five times for parallel pipes due to the unfavorable static pressure distribution along the length of the exchanger. Amanowicz [4] combined computational fluid dynamics (CFD) with 1:4 scale experiments and demonstrated that a switch from Z to U supply arrangement led to the reduction in overall pressure losses by between 6%–36%, respectively, while increasing airflow uniformity by 80%.

These studies highlight that layout and manifold choices are not minor details: they directly control flow maldistribution and pressure losses, and therefore influence the net energy benefit once fan power is considered.

The thermal performance has been analyzed under varied environments and conditions of operation. Ahmed et al. [5] studied a grid Earth-to-Air Heat Exchanger in the hot, humid Australian climate. In their work the dimensions of the PVC pipe were 0.02 m in diameter and 7.5 m long. The average temperature drop was 4.11°C, proving the influence of pipe diameter, pipe length, and flow rate. Sakhri et al. [6] presented experimental research in a desert area of Southwest Algeria with an increase in temperature of 13°C during heating and a decrease of 7°C when cooling, as well as considerable local climatic-condition effects. Ahmad and Prakash [7] experimented on the EAHE system with PVC pipes of three diameters in the range of 0.0285–0.0485 m, and the inlet airflow velocity is in the range of 2 to 6.5 m/s. They reported that a higher temperature difference $\Delta T$ occurs for smaller diameters, whereas an increase of inlet velocity resulted in a slight reduction from the heating or cooling profile within the matrix heat exchanger. They also found that EAHE effectiveness ($\varepsilon$) decreases with velocity and is lower for larger diameters; however, heating/cooling capacity increases with inlet velocity.

Overall, experimental results across climates consistently show that the thermal response depends strongly on airflow rate and pipe sizing, while the achievable temperature change is highly site-dependent (ambient conditions and soil coupling). This makes greenhouse applications in hot regions particularly sensitive to both thermal performance and ventilation demand.

Numerical and modeling approaches have commonly been applied to estimate the performance of EAHE under various operating conditions. A performance evaluation is given for a system, focusing on the pipe material and thickness variations described by Hasan and Noori [8]. According to their study, the use of PVC is advantageous from both the economic and the anticorrosion points of view, while also highlighting the effects of varying air conditions. Hasan and Noori [9] studied single-layer and double-layer buried EAHE systems based on the analysis used for predicting annual energy saving rates, where a considerable decrease in annual energy consumption is achieved when a double layer of an EAHE is used. Mohammed et al. [10] developed a MATLAB/Simulink model to simulate various configurations. They concluded that multi dividual pipes worked not only better for cooling but also for the pressure-loss reduction. Hasan and Eman [11] studied the effect of the disturbed soil thickness around the pipes on the stable wall at low wind speed and the disturbed layer thickness in the range of 1d to 6d using a CFD for Nasiriya city, Iraq.

Collectively, the modeling studies highlight that material and configuration (single or multi-pipe, single versus multiple courses) and the behavior of soil–pipe thermal interaction assumed could bias predicted performance; however, practical benefits depend on how well models capture real soil conditions and pressure-loss penalties.

Recent peer-reviewed research in the 2023–2025 period has strengthened even further the empirical underpinning of EAHE systems and provided specific design recommendations for hot, arid regions as well as for greenhouses. Notably, Hegazy and Mohamed [12] introduced a remote-sensing-driven screening framework for Egypt's New Delta and highlighted that ground temperatures at roughly 4 m depth can exhibit only modest fluctuations. This result further justifies the selection of installation depths in this range—particularly in arid, data-scarce environments where remote sensing can offer useful large-area guidance for substantively guiding siting and design decisions. In a similar vein, Sakhri et al. [13] studied the thermal and economic analysis of the EAHE applied to an indoor climate conditioning system during winter in arid regions as a low-$CO_2$ conditioning technique. For CEA, Nauta et al. [14] integrated an EAHE in a commercial greenhouse energy model and demonstrated that key design choices—most importantly the depth of burial and fan operation conditions—are mainly responsible for large-scale energy efficiency outcomes. Finally, Sofyan et al. [15] simulated CFD to compare between series and parallel configurations, based on which it was suggested that selection of the configuration does not only take care of thermal gains but also takes into account the penalty due to pressure loss.

In conclusion, previous studies have significantly improved the insight on EAHE systems and their design parameters. However, the experimental research into the thermal and hydraulic performance of EAHEs in practical greenhouses is relatively limited. In particular, fewer studies jointly report the EAHE outlet air temperature delivered to the greenhouse and the associated pressure losses/fan energy under repeatable operating conditions, which is essential for assessing the net benefit in hot climates.

This study examined the thermal performance and energy efficiency of an EAHE system within a greenhouse, providing a practical environment to evaluate its effectiveness in hot climate regions. The results enhance passive cooling techniques in thermal systems engineering and demonstrate the effectiveness of EAHE systems for energy-efficient greenhouse air conditioning in elevated temperatures.

To synthesize the governing trends reported across EAHE studies, Table 1 summarizes the main design/operational factors and their reported effects.

**Table 1.** Synthesis of key governing trends reported across Earth-Air Heat Exchanger (EAHE) studies

| Ref. | Climate/ Location | Configuration/ Focus | Method | Key Governing Trend (Synthesis) |
|---|---|---|---|---|
| [1] | Poznań Poland (lab-scale) | Multi-pipe EAHE (U- and Z-type); flow nonuniformity. | Modeling and analysis | Minor geometry changes improved flow uniformity and increased heat transfer by $\sim 9\%$, indicating coupled thermal-hydraulic behavior. |
| [2, 3] | Poznań Poland (lab-scale) | Manifold design/configuration in parallel pipes. | CFD + experiments | Manifold static-pressure distribution dominated flow allocation (up to $\sim 5\times$ differences), strongly affecting performance. |
| [4] | Poznań Poland (lab-scale) | Supply arrangement (Z vs. U) in multi-pipe EAHE. | CFD + 1:4 scale experiments. | Switching the supply layout ( Z to U ) reduced total pressure losses by $6\% - 36\%$ and improved airflow uniformity by up to $\sim 80\%$, demonstrating geometry-driven $\Delta P$ penalties. |
| [5] | Australia (hot-humid) | Grid-type EAHE; PVC pipe (D = 0.02 m, L = 7.5 m). | Experimental | Cooling performance depended on pipe sizing and airflow rate; average $\Delta T \approx 4.11^{\circ}\mathrm{C}$, indicating sensitivity to D, L, and flow. |
| [6] | Southwest Algeria (arid) | EAHE operation in heating/cooling modes. | Experimental | Local climate strongly affected achievable temperature change ($\approx +13^{\circ}\mathrm{C}$ in heating; $\approx 7^{\circ}\mathrm{C}$ in cooling). |
| [7] | Patna, India (controlled test rig) | Experimental EAHE test rig; three PVC pipe diameters at different inlet velocities (heating and cooling). | Experimental | Smaller diameters yield larger temperature change ($\Delta T$); increasing inlet velocity slightly reduces $\Delta T$, while heating/cooling capacity increases with velocity; effectiveness decreases with velocity and is lower for larger diameters. |
| [8] | Nasiriya, Iraq (hot climate) | Pipe material and thickness effects. | Modeling and analysis | Material choice influenced feasibility (PVC offered economic and anticorrosion advantages); inlet air conditions affected predicted performance. |
| [9] | Nasiriya, Iraq (hot climate) | Single-laver vs double-layer buried EAHE. | Modeling + annual energy analysis | Configuration affected annual savings; double-layer arrangements reduced annual energy use relative to a single-layer layout. |
| [10] | Kufa, Iraq (hot climate) | Various configurations; multi-single pipe systems. | MATLAB/ Simulink modeling | Configuration shifted the cooling-$\Delta P$ trade-off, multi-single pipe systems improved cooling while reducing pressure losses. |
| [11] | Nasiriya, Iraq (hot climate) | Disturbed-soil thickness around pipe (1d–6d) at low airflow velocities. | CFD and analysis | Soil-pipe thermal interaction was goveming; disturbed-soil thickness (1d–6d) altered stabilized wall temperature and heat exchange. |

| Ref. | Climate / Location | Configuration / Focus | Method | Key Governing Trend (Synthesis) |
|---|---|---|---|---|
| [12] | Egypt (arid regions /New Delta) | Remote-sensing screening for EAHE feasibility (depth). | Peer-reviewed journal (Scientific Reports) | Data-driven screening supported feasibility assessment where subsurface profiles were limited; modest temperature variation around $\sim$ 4m depth supported this installation range. |
| [13] | Arid winter environments | Thermal + economic performance for indoor climate control. | Peer-reviewed journal (Int. J. Low-Carbon Technologies) | Recent work linked thermal performance with economic assessment, reinforcing EAHE as a low-carbon conditioning option in arid climates. |
| [14] | Canada | EAHE integrated into greenhouse energy model. | Peer-reviewed journal (Journal of Biosystems Engineering) | At greenhouse scale, net energy impact was sensitive to key design/operating variables; simulations identified feasible depth/flow ranges and expected energyefficiency outcomes. |
| [15] | Not specified (CFD comparative study) | Series vs parallel EAHE arrangements (thermal $+\Delta P$). | Peer-reviewed journal (Results in Engineering) | Configuration selection should reflect the thermal-hydraulic trade-off; temperature change alone is insufficient without $\Delta P$/fan-energy penalties. |

## 2 Methodology

### 2.1 Problem Description

This paper investigated the thermal and hydraulic performance of an EAHE system designed in a U-type configuration. The exchanger consisted of six parallel, side-by-side PVC pipes. Each pipe was 6.93 m long, with a total pipe length of 53 m. The manifold and branch pipe diameters were 0.1016 m. The system was installed at a depth of 3.5 m, as indicated in Figure 1.

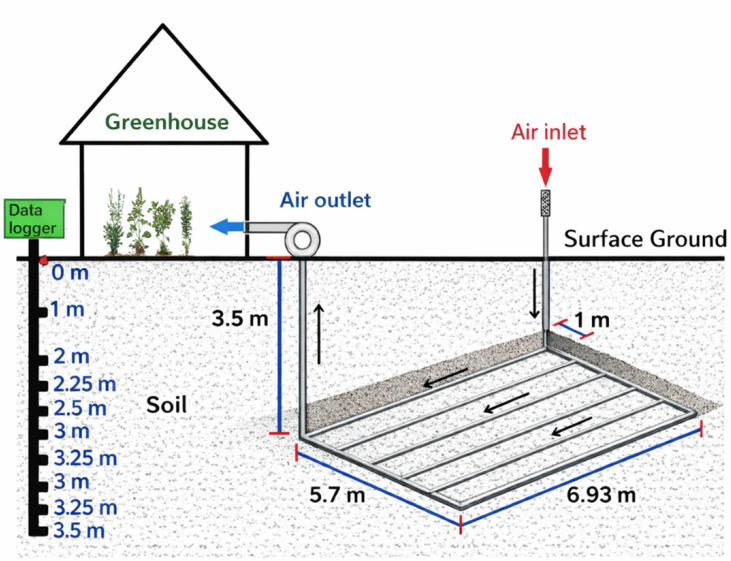


**Figure 1.** Schematic of the U-type EAHE system

This study primarily comprised an experimental field investigation conducted under the climatic conditions of Nasiriyah (Southern Iraq) to quantify the thermal and hydraulic performance of a U-type EAHE. To support the experimental analysis, a CFD model was developed in ANSYS 2024 to verify the physical consistency of the measured trends and to examine flow distribution and pressure-loss characteristics that are not easily accessible through measurements alone. Based on the experimental dataset, the system was evaluated using key performance

indicators, including total pressure drop, fan power demand, thermal effectiveness, heat transfer rate, and an overall performance factor. This set of metrics enabled a comprehensive assessment of EAHE performance.

### 2.2 Experimental Setup

An experimental study was conducted in the current research on a grid-type, U-configuration EAHE system to determine thermal and hydraulic performance. The exchanger included six PVC pipes arranged in parallel. The pipe length and diameter were 6.93 m and 0.1016 m, respectively (see Figure 2a, Figure 2b), and the total pipe length was approximately 53 m. The same pipe diameter was used for the header and the parallel pipes. The system was buried at a depth of 3.5 m (Figure 2c).

A small greenhouse was built for the experimental site (Figure 2e) so that measurements were conducted under real operating conditions. A variable-speed fan was installed at the outlet section to circulate air through the EAHE system, as shown in Figure 3. System temperature was recorded using fourteen K-type thermocouples. Two sensors were installed at the air intake and exhaust of the heat exchanger, and two additional sensors were installed in the middle of the greenhouse interior. One thermocouple was used to measure ambient air temperature. The remaining sensors were vertically installed in a PVC pipe to measure soil temperature at different depths up to 3.5 m, as depicted in Figure 4 and Figure 5.

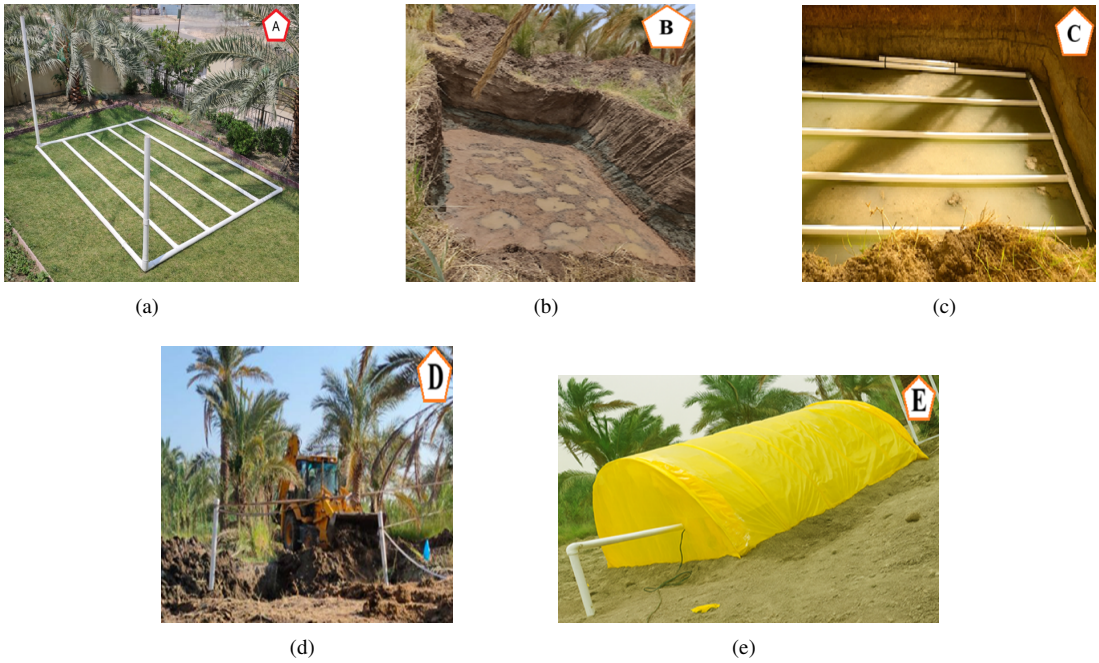


(a) (b) (c)

(d) (e)

**Figure 2.** Main construction stages of the experimental EAHE set-up: (a) installation of the PVC pipe network; (b) excavation of the 8 × 7 × 3.5 m pit; (c) placement and leveling of the pipes; (d) backfilling of the pit; (e) connection of the EAHE to the greenhouse


**Figure 3.** Variable-speed fan used to drive airflow through the EAHE pipes

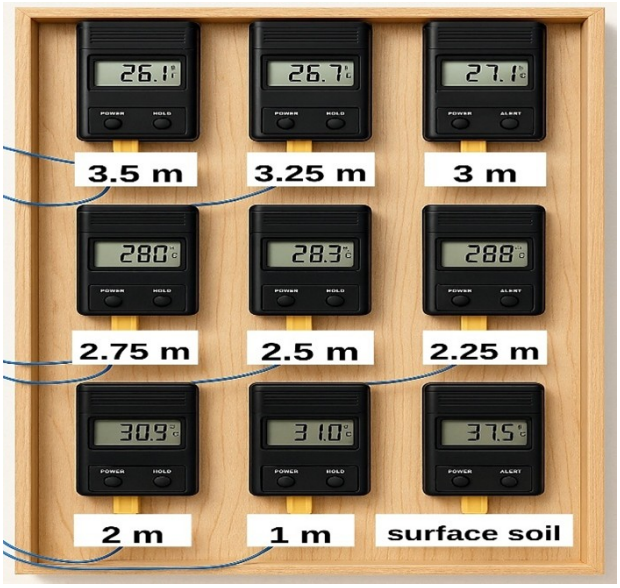


**Figure 4.** Soil profile and locations of the thermocouple sensors along the 3.5 m

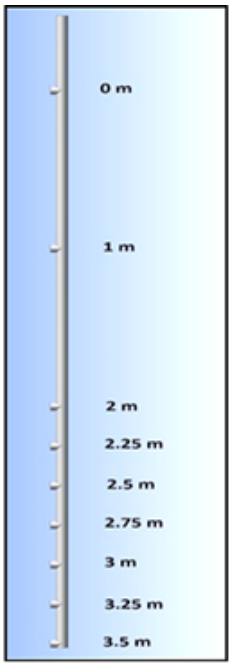


**Figure 5.** PVC pipe assembly housing the temperature sensors at different soil depths

Air pressure and velocity at the inlet and outlet were measured using a FLUKE 922 airflow meter (Figure 6). Temperature data were recorded at 30-min intervals under steady-state conditions using an Extech TM500 12-channel temperature datalogger (Figure 7). All instruments were calibrated prior to the experiments to ensure measurement accuracy and reliability.

The experiments were performed over the period of July–October 2025 with airflow velocities at 11, 13, 15, and 17 m/s. Each airflow velocity level (n = 3) runs on three separate days. After steady operation was reached, the value of inlet and outlet air temperatures ($Ti$, $To$) was registered every 30 min. A daily average was calculated from the steady-period readings and presented as the mean $\pm$SD of these 3 daily averages. The total pressure drop ($\Delta P$) was measured as a steady-state spot reading for each velocity because the differential pressure meter provides instantaneous readings without data logging. Therefore, $\Delta P$ was reported as a single value with instrument accuracy: $\pm$(1% of reading + 1 Pa). The recorded data were post-processed to identify key performance parameters, including thermal effectiveness ($\varepsilon$), total pressure loss, and overall efficiency factor ($\eta$*). The experimental data were then compared with CFD simulations to verify the model.


**Figure 6.** FLUKE 922 airflow meter used to measure air velocity and differential pressure at the EAHE inlet and outlet


**Figure 7.** Extech TM500 12-channel thermocouple data logger used to monitor temperature variations

### 2.2.1 Uncertainty and error analysis

Air temperature was measured using Type-K thermocouples connected to an Extech TM500 12-channel data-logging thermometer (resolution: 0.1°C; basic accuracy: ±0.4% of reading ±1°C for Types J/K/E/T). Air velocity and differential pressure were measured using a Fluke 922 micromanometer (velocity accuracy: ±2.5% of reading; pressure accuracy: ±(1% of reading + 1 Pa)).

The uncertainty in the temperature difference was estimated using:

$$u_{\Delta T} = \sqrt{{u_{T_i}}^2 + {u_{T_o}}^2} \tag{1}$$

Instrument resolutions and accuracies are summarized in Table 2.

**Table 2.** Measurement instruments, resolution, and accuracy

| Quantity | Instrument | Resolution | Accuracy |
|---|---|---|---|
| Temperature (°C) | Extech TM500 (Type-K) | 0.1°C | ±0.4% of reading ±1°C |
| Air velocity (m/s) | Fluke 922 | 0.001 m/s | ±2.5% of reading |
| Differential pressure (Pa) | Fluke 922 | 1 Pa | ±1% of reading +1 Pa |

### 2.3 Mathematical Model

#### 2.3.1 Assumptions

To keep the problem analytically tractable, several simplifying assumptions were adopted in the mathematical model [16]:

1. The process was steady-state.
2. The flow was steady and uniform throughout the entire domain.
3. Soil properties were uniform and homogeneous.
4. The airflow was subsonic (M $<$ 0.3); therefore, it was treated as incompressible with constant thermal conductivity, density, and specific heat capacity.
5. Perfect thermal contact existed between the pipe wall and the surrounding soil.
6. A turbulent flow regime (Re $>$ 4000) was assumed inside the pipe, and the corresponding turbulent correlations were applied.

#### 2.3.2 Governing equations and performance parameters

Although the governing equations are standard, the novelty of this work lies in the validated 3D conjugate heat-transfer CFD model developed for a multi-pipe U-type EAHE under representative hot-climate boundary conditions. The underlying fluid-flow and heat-transfer equations follow the standard formulations reported in [17].

• Continuity equation:

$$\frac{1}{r}\frac{\partial}{\partial r}(rv_r) + \frac{1}{r}\frac{\partial}{\partial \theta}v_\theta + \frac{\partial}{\partial z}v_z = 0 \tag{2}$$

• Momentum equations:

$r$-direction:

$$\frac{\partial v_r}{\partial t} + (v\cdot\nabla)v_r - \frac{v_\theta^2}{r} = -\frac{1}{\rho}\frac{\partial p}{\partial r} + v\left[\Delta v_r - \frac{v_r}{r^2} - \frac{2}{r^2}\frac{\partial v_\theta}{\partial \theta}\right] + g_r \tag{3}$$

$\theta$-direction:

$$\frac{\partial v_\theta}{\partial t} + (v\cdot\nabla)v_\theta + \frac{v_r v_\theta}{r} = -\frac{1}{\rho r}\frac{\partial p}{\partial \theta} + v\left[\Delta v_\theta - \frac{v_\theta}{r^2} + \frac{2}{r^2}\frac{\partial v_r}{\partial \theta}\right] + g_\theta \tag{4}$$

$z$-direction:

$$\frac{\partial v_z}{\partial t} + (v\cdot\nabla)v_z = -\frac{1}{\rho}\frac{\partial p}{\partial z} + v\Delta v_z + g_z \tag{5}$$

• Energy equation:

$$\rho c_p\left(\frac{\partial T}{\partial t} + (v\cdot\nabla)T\right) = k\Delta T + \Phi \tag{6}$$

• Performance calculations:

The following equations are used to evaluate the performance of the EAHE system [12, 18, 19]:

$$\varepsilon = \frac{(T_i - T_o)}{(T_i - T_s)} \tag{7}$$

$$A = \frac{\pi}{4}d^2 \tag{8}$$

$$\dot{m} = \rho v A \tag{9}$$

$$Q_{EAHE} = \dot{m} c_p \left(T_i - T_o\right) \tag{10}$$

$$\Delta P_{tot} = p_i - p_o \tag{11}$$

$$\dot{V} = \frac{\dot{m}}{\rho} \tag{12}$$

$$P.P = \dot{V} \Delta P_{\text{tot}} \tag{13}$$

$$\eta^* = \frac{Q_{EAHE}}{P.P} \tag{14}$$

#### 2.3.3 Boundary conditions

The following boundary conditions were introduced to build the mathematical model:

• Inlet boundary condition

At the inlet of the EAHE, constant velocities of 11, 13, 15, and 17 m/s were defined to represent different airflow rates. The dry-bulb temperature ($Ti$) was also specified. The inlet was treated as turbulent, subsonic flow. The inlet temperatures were obtained from real climatic data for Nasiriya city, southern Iraq, during the summer season.

• Outlet boundary condition

A constant zero-gauge pressure was assigned at the outlet, while the exit temperature was obtained from the numerical solution.

• Wall boundary condition

The horizontal portion of the EAHE pipes was modeled as thermally coupled to the disturbed soil. Therefore, a conjugate heat-transfer method was applied at this interface to represent heat exchange among the air, pipe wall, and surrounding soil. Beyond the disturbed-soil layer, at a distance ($\delta$) from the pipe wall, soil temperature was assumed constant and equal to the undisturbed ground temperature ($T_s$ = 26.1°C), This value was experimentally measured at a depth of 3.5 m (Figure 4) and was also reported for the study area in [20]. To simplify the numerical model, the short near-surface vertical inlet/outlet sections were treated as thermally insulated. Because these segments are short and temperature changes occur in opposite directions (cooling in the inlet leg and warming in the outlet leg), their net influence on the outlet temperature is expected to be small compared with the horizontal buried pipe at 3.5 m depth, where soil temperature is relatively stable. This treatment is consistent with common practice in EAHE simulations [11, 19, 21]; however, it remains a simplification that may introduce a small bias.

### 2.4 Numerical Solution

The governing equations were solved numerically using the finite volume method. The CFD approach was adopted to solve the three-dimensional Navier–Stokes equations together with the continuity equation.

#### 2.4.1 CFD modeling

In recent years, CFD has been widely used to model and evaluate the performance of EAHE systems [22]. In this study, airflow through the EAHE pipes was simulated under the prescribed boundary conditions using CFD. The simulations were performed using ANSYS Fluent 2024. The standard k-$\varepsilon$ turbulence model with standard wall functions was applied to simulate the flow. The energy equation was also enabled to account for heat transfer among the flowing air, pipe wall, and surrounding soil.

The CFD approach allowed determination of airflow characteristics at different locations within the EAHE system. These locations were discretized using a numerical mesh. Convergence was assumed when the residuals of the momentum and energy equations were less than $1\times10^{-6}$.

#### 2.4.2 Mesh independence assessment

A mesh-independence study was performed to ensure that the numerical predictions were not affected by mesh resolution. In general, refining the mesh (i.e., using smaller elements) increases the number of elements and improves flow-field resolution, which typically leads to more accurate CFD predictions; however, it also increases computational cost.

Table 3 summarizes the relationship between the mesh number, the number of elements, and the resulting outlet air temperature ($T_o$) of the EAHE. Figure 8 shows the outlet air temperature distribution for different mesh densities. The results indicate that the solution became effectively mesh independent at the selected refinement level, as $To$ changed negligibly when the mesh was refined from Mesh 3 to Mesh 4 ($\Delta T_o \approx 0.0004$ K). Therefore, Mesh 3 was selected because it offers a practical balance between accuracy and computational effort.

**Table 3.** Mesh independent check

| Mesh Number | $T_o$(K) | Element Number |
|---|---|---|
| Mesh 1 | 303.5023 | 2114606 |
| Mesh 2 | 302.4753 | 2819475 |
| Mesh 3 | 302.4362 | 4232488 |
| Mesh 4 | 302.4358 | 8458425 |

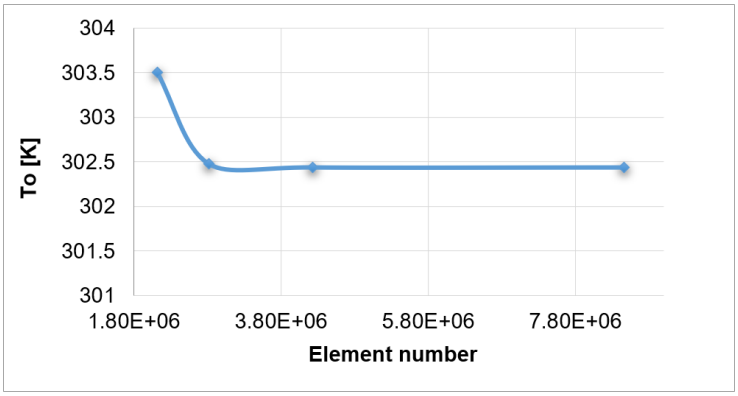


**Figure 8.** Effect of mesh density (number of elements) on the predicted EAHE outlet air temperature

2.4.3 Validation of the simulation model

The current experiments were implemented under the climate of Nasiriyah, southern Iraq, during the July-October period. The inlet air temperature ranged from 35°C to 54°C, while the soil temperature at a depth of 3.5 m remained nearly constant at about 26.1°C. The system consisted of a grid of six buried PVC pipes, each 6.93 m long with an internal diameter of 0.1016 m, giving a total pipe length of 53 m. It was assumed that the thermophysical properties of air and soil remained constant [19], as listed in Table 4.

**Table 4.** The thermophysical properties of air and soil [19]

| Material | Density (kg/m$^3$) | Specific Heat (J/kg·°C) | Thermal Conductivity (W/m·°C) |
|---|---|---|---|
| Air | 1.225 | 1007 | 0.0242 |
| Saturated soil | 2000 | 880 | 1.4 |
| PVC | 1380 | 900 | 0.16 |

Figure 9 compares the measured outlet air temperature with CFD predictions at airflow velocities of 11, 13, 15, and 17 m/s. The model followed the experimental trend well. Using ASHRAE Guideline 14 hourly indices computed from 30-min data over 72 h for each velocity, the agreement was quantified using CV(RMSE) and NMBE (definitions below). The model yielded CV(RMSE) = 9.05% and NMBE = 9%, satisfying the ASHRAE hourly criteria ($\leq$30% and $\leq$10%, respectively). The ASHRAE error indices were computed as [23]:

$$RMSE = \sqrt{\frac{1}{n}\sum_{i=1}^{n}\left(T_{o,CFD,i} - T_{o,Exp,i}\right)^2} \tag{15}$$

$$CV(RMSE) = \frac{RMSE}{\bar{T}_{o,Exp}} \times 100\% \tag{16}$$

$$NMBE = \frac{\sum_{i=1}^{n}\left(T_{o,Exp,i} - T_{o,CFD,i}\right)}{(n-1)\times \bar{T}_{o,Exp}} \times 100\% \tag{17}$$

where, $n$ is the number of 30-min samples collected over 72 h for each velocity. For context, published EAHE validation studies report deviations ranging from about 3%–4% in controlled tests [24] to 7.46% under transient operation [25]. In tunnel-scale studies, deviations have reached up to 11.70% for outlet temperature, while the

maximum difference in total pressure drop was about 14% [26]. In addition, comparisons against the dataset of Hegazy et al. [27] show temperature-drop differences of 2.4%–14.8%, depending on velocity and modeling assumptions. The remaining underprediction in the present work was most likely due to simplifying assumptions (e.g., constant thermophysical properties and simplified treatment of the vertical inlet/outlet sections).

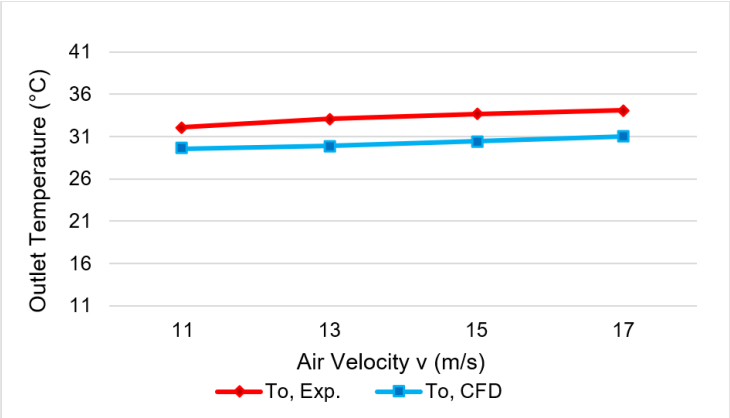


**Figure 9.** Variation of outlet air temperature (°C) predicted numerically and measured experimentally at different airflow velocities

To complement the graphical validation, Table 5 summarizes the agreement between CFD predictions and experimental measurements across the four tested inlet velocities. The comparison focuses on outlet air temperature and total pressure drop, which directly govern cooling performance and fan-power demand.

**Table 5.** CFD-experiment validation summary for outlet temperature and total pressure drop

| v (m/s) | $\Delta P$_Exp (Pa) $\pm$ $u_{\Delta P}$ | $\Delta P$_CFD (Pa) | $\Delta P$ Abs. Deviation (%) | $T_o$_Exp (°C) $\pm$ SD | $T_o$_CFD (°C) | $\Delta T_o$ (°C) | $T_o$ Abs. Deviation (%) |
|---|---|---|---|---|---|---|---|
| 11 | $475 \pm 5.8$ | 410 | 13.7% | $32.08 \pm 0.12$ | 29.52 | 2.56 | 8.0% |
| 13 | $670 \pm 7.2$ | 565 | 8.9% | $33.11 \pm 0.48$ | 29.95 | 3.16 | 9.5% |
| 15 | $870 \pm 9.1$ | 743 | 8.6% | $33.62 \pm 0.52$ | 30.49 | 3.13 | 9.3% |
| 17 | $1047 \pm 11.5$ | 951 | 9.2% | $34.11 \pm 0.19$ | 30.95 | 3.16 | 9.3% |

Overall, the model captured the experimental trends with velocity while showing a consistent underprediction of $T_o$ and $\Delta P$ within the reported deviations. These systematic differences are discussed in light of the modeling assumptions and measurement limitations in the following subsection.

### 2.4.4 Influence of assumptions

The CFD model was based on steady-state operation, homogeneous soil conditions, and constant thermophysical properties. In practice, soil temperature and moisture can vary with depth, location, and time, and the soil adjacent to the pipe can gradually warm during prolonged operation. Neglecting these effects can make the model overly idealized and can lead to biased heat-exchange predictions. In the present case, the simplifying assumptions contributed to systematically lower predicted outlet temperatures ($T_o$) than those measured.

Treating the short near-surface vertical inlet/outlet segments as thermally insulated was another simplifying assumption. A refined treatment that accounts for near-surface thermal interaction could be examined in future work. In addition, the underprediction of total pressure drop ($\Delta P$) may be partly attributable to simplified representations of wall roughness and minor losses in the manifold and branch junctions. Incorporating transient behavior, moisture- and depth-dependent soil properties, and a more detailed treatment of distributed and local losses would likely reduce these discrepancies.

## 3 Results and Discussion

This section first presents the thermal performance of the EAHE–greenhouse system and then quantifies the associated hydraulic penalty. Next, the thermal–hydraulic trade-off is synthesized. CFD results are also used as internal diagnostics to support interpretation of the experimental findings.

### 3.1 Thermal Performance of the EAHE–Greenhouse System

Figure 10 shows the average diurnal temperature profiles of the ambient air ($Ti$), the EAHE outlet air ($To$), and the greenhouse air ($Tg$) for the period July–October. The ambient temperature follows a typical diurnal cycle, increasing from about 40°C in the morning to nearly 50°C around noon and then decreasing in the afternoon. In contrast, the EAHE outlet temperature is considerably lower and relatively stable (32–36°C), reflecting the thermal buffering of subsurface soil and attenuation of daily fluctuations. The greenhouse air temperature remains between $Ti$ and $To$, indicating that the EAHE-assisted ventilation system moderates the indoor environment.

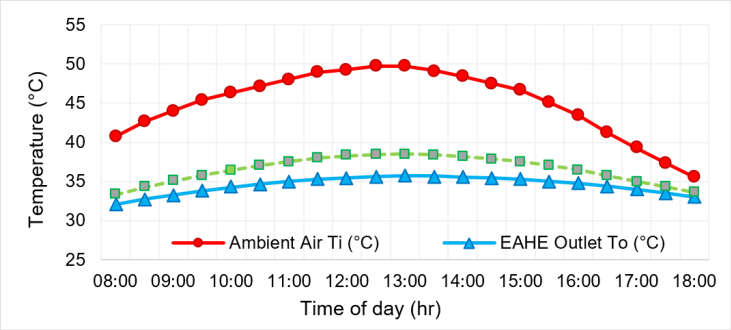


**Figure 10.** Average diurnal temperature profiles of ambient air ($T_i$), EAHE outlet air ($T_o$), and greenhouse air ($T_g$) from July to October

During peak hours (11:00–16:00), the average cooling relative to ambient air is about 9°C, which provides a representative measure of typical daily performance. $T_o$ is relatively stable during this period, and the temperature difference between greenhouse air and EAHE outlet air is 2–3°C; this phenomenon implies that stable operation can be obtained under high thermal loads. In summary, Figure 10 indicates that the EAHE maintains reasonably stable and acceptable temperature conditions over the period of analysis.

Figure 11 presents the relationship between ambient air temperature ($T_i$) and greenhouse air temperature ($T_g$) under daytime conditions. The data are highly linear, indicating that changes in ambient conditions translate to the greenhouse response, but with attenuation. The slope of the fitted regression line is less than unity, showing that the greenhouse heats up at a lower rate than the ambient air due to damping provided by the EAHE-assisted ventilation system. For example, as $Ti$ increases from 46°C to 54°C, $Tg$ increases only from about 38.8°C to 41°C (≈2.2°C), corresponding to ∼25%–30% of the ambient increase. Over the same range, the $T_i - T_g$ difference remains substantial (approximately 7–13°C). Small departures from the regression line can be attributed to temporal variations in solar radiation and/or airflow rate. In general, Figure 11 substantiates that the EAHE provides a reasonable capacity to maintain a favorable indoor climate under severe summer conditions.

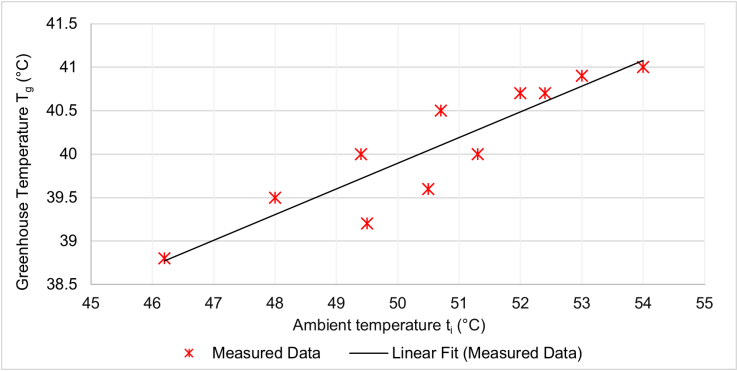


**Figure 11.** Relationship between ambient air temperature ($T_i$) and greenhouse air temperature ($T_g$) during daytime operation

Figure 12 depicts the monthly average cooling potential, $\Delta T = (T_i - T_o)$, at 14:00. $\Delta T$ decreases gradually from 15.9°C in July to 13.5°C in October (Table 6). This seasonal decrease is mainly related to milder external conditions and gradual thermal equilibration between the surrounding soil (3.5 m depth) and the air flowing through the pipes toward the end of the hot season. Nevertheless, the EAHE maintains a cooling potential greater than 13°C throughout all months, indicating stable precooling capability compatible with greenhouse ventilation and energy-efficient operation over the cooling period.

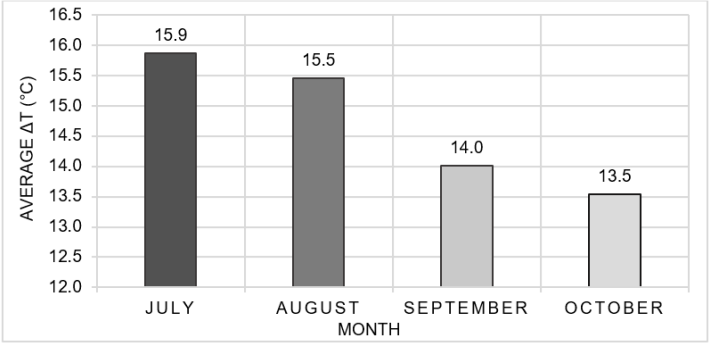


**Figure 12.** Monthly variation of the EAHE cooling potential ($\Delta T = T_i - T_o$) at 14:00

**Table 6.** Monthly mean of cooling potential at 14:00

| Month | Average Ambient Air Temperature ($T_i$, °C) | EAHE Outlet Temperature ($T_o$, °C) | Temperature Difference ($\Delta T$, °C) |
|---|---|---|---|
| July | 51.05 | 35.18 | 15.9 |
| August | 51.11 | 35.65 | 15.5 |
| September | 48.76 | 34.75 | 14.0 |
| October | 46.13 | 32.60 | 13.5 |

Figure 13 shows the variation of thermal effectiveness ($\varepsilon$) with airflow velocity. $\varepsilon$ decreases from 0.75 at 11 m/s to 0.68 at 17 m/s, mainly due to reduced residence time inside the buried pipes, which limits heat exchange with the surrounding soil. However, $\varepsilon$ remains above 0.68 across all tested velocities, indicating stable heat-transfer capability. Therefore, a moderate inlet airflow velocity (13–15 m/s) provides a practical balance between cooling performance and the aerodynamic/pressure-drop behavior discussed above.

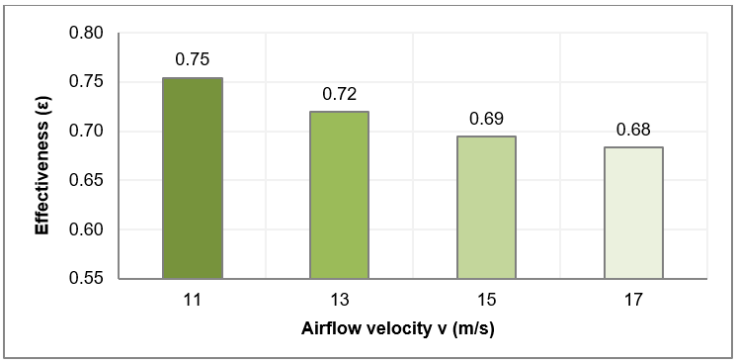


**Figure 13.** Thermal effectiveness ($\varepsilon$) of the EAHE as a function of airflow velocity

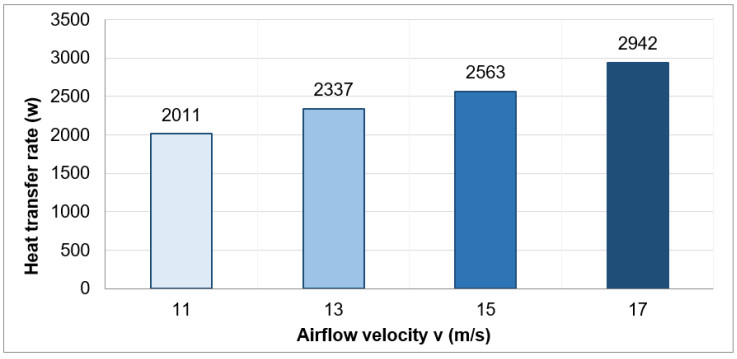


**Figure 14.** Sensible cooling power ($Q_{\text{EAHE}}$) variation with airflow velocity

Figure 14 presents the sensible cooling power ($Q_{\mathrm{EAHE}}$) as a function of airflow velocity $Q_{\mathrm{EAHE}}$ increases nearly linearly from about 2.0 kW at 11 m/s to about 2.9 kW at 17 m/s due to higher mass flow rate and enhanced convective heat transfer. At higher velocities (above 15 m/s), $\Delta T$ decreases slightly because of reduced residence time. Consequently, although $Q_{\mathrm{EAHE}}$ continues to rise, the overall performance per unit fan power tends to decline, indicating that moderate flow rates offer a better thermal–energy trade-off.

While the above results describe the delivered cooling benefit, the practical operating range also depends on the corresponding pressure drop and fan-power requirement, which are discussed next.

### 3.2 Hydraulic Performance: Pressure Drop and Fan Power

Figure 15 presents the measured total pressure drop across the EAHE ducts ($\Delta P_{\mathrm{tot}}$) as a function of airflow velocity. As velocity increases from 11 m/s to 17 m/s, $\Delta P_{\mathrm{tot}}$ increases nonlinearly from about 475 Pa to more than 1000 Pa. This trend is consistent with turbulent flow, where frictional losses dominate and pressure drop scales approximately with the square of velocity. At higher velocities, the large increase in $\Delta P_{\mathrm{tot}}$ translates to an appreciable increase in fan power, highlighting the importance of balancing airflow rate and energy efficiency in system design and operation.

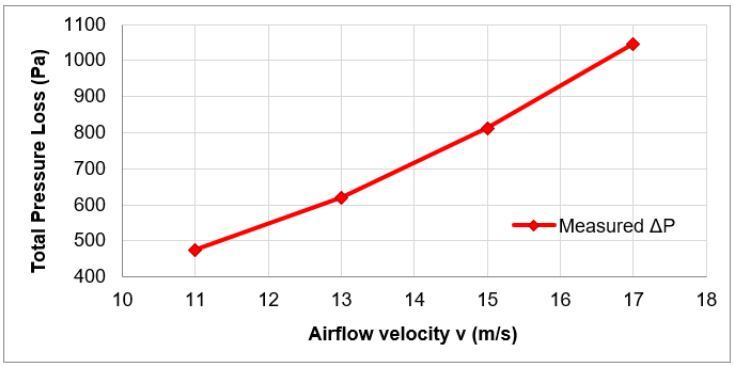


**Figure 15.** Variation of total pressure drop ($\Delta P_{\mathrm{tot}}$) across the EAHE pipes with airflow velocity

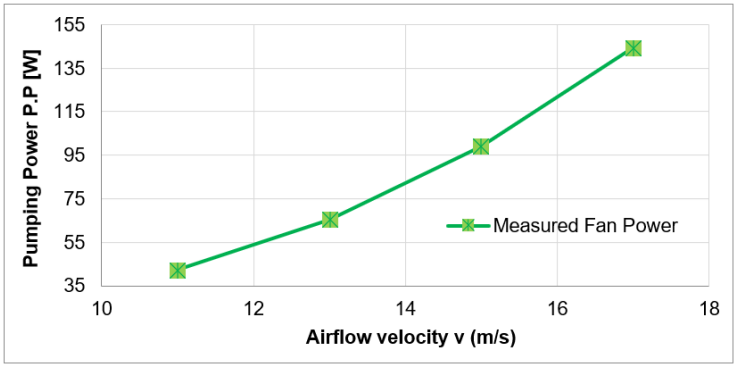


**Figure 16.** Fan power consumption as a function of airflow velocity inside the EAHE pipes

**Table 7.** Average thermal and hydraulic performance by airflow velocity

| Air Velocity (m/s) | Pressure Drop ($\Delta P$, Pa) | Fan Power (W) | $T_o$ Mean $\pm$ SD (°C) (n = 3) | Cooling Power ($Q_{\mathrm{EAHE}}$, W) | Effectiveness ($\varepsilon$) | Overall Performance ($\eta^*$) |
|---|---|---|---|---|---|---|
| 11 | 475 | 42.4 | $32.08 \pm 0.12$ | 2011 | 0.75 | 47.4 |
| 13 | 670 | 70.1 | $33.11 \pm 0.48$ | 2337 | 0.72 | 35.8 |
| 15 | 870 | 110.8 | $33.62 \pm 0.52$ | 2563 | 0.69 | 25.9 |
| 17 | 1047 | 144.4 | $34.11 \pm 0.19$ | 2942 | 0.68 | 20.4 |

Note: $T_o$ values are reported as mean $\pm$SD across three independent days (n = 3), where each day's value is the average of 30-min steady-operation readings (Section 2.2).

Figure 16 shows the fan power as a function of airflow velocity. For velocities between 11 and 17 m/s, fan power increases strongly from about 42 W to nearly 145 W (Table 7), showing an approximately cubic dependence on velocity. At higher velocities, increased frictional and dynamic losses in the buried pipes lead to higher energy consumption. This behavior emphasizes the need to select moderate inlet airflow rates to achieve effective cooling while maintaining energy savings.

### 3.3 Thermal-Hydraulic Trade-Off and Recommended Operating Range

Figure 17 displays the overall performance index ($\eta$*), defined as the ratio of useful cooling power to fan input power. $\eta$* decreases from 47.4 at 11 m/s to 20.4 at 17 m/s because fan power increases much faster than EAHE cooling capacity. Although EAHE heat transfer increases with airflow velocity, fan power increases approximately with the cube of velocity, which reduces overall performance. This behavior indicates a clear thermal–hydraulic trade-off: higher velocity enhances cooling, but it incurs substantial energy penalties. Therefore, the 13–15 m/s range provides a practical balance between cooling performance and electrical demand.

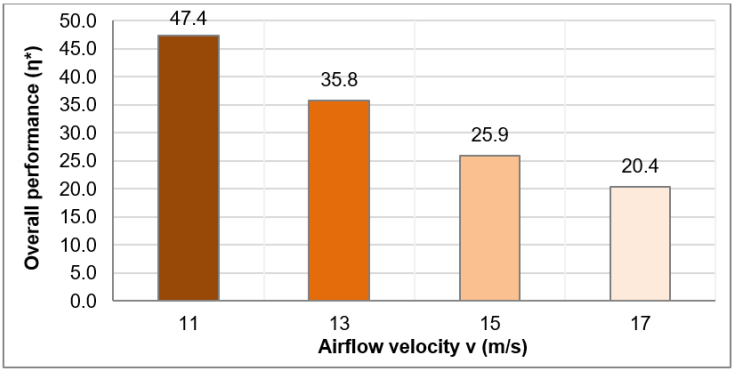


**Figure 17.** Overall performance index ($\eta$*) of the EAHE system versus airflow velocity

To connect the recommended operating range to the underlying flow mechanisms, the CFD model was used as a diagnostic tool to examine the internal pressure field and branch-wise flow distribution under representative operating conditions.

### 3.4 CFD Diagnostics Supporting the Experimental Interpretation ($v_i$ = 15 m/s)

Figure 18 shows a gradual decrease in static pressure from the inlet manifold toward the outlet, with no sharp high-gradient regions along the main flow path. This indicates that the overall pressure drop is mainly associated with distributed losses along the manifold and branches, with additional contributions from junctions and bends. The smooth pressure field also provides a physical basis for the experimentally observed increase in total $\Delta P$ and fan-power demand as airflow velocity increases.

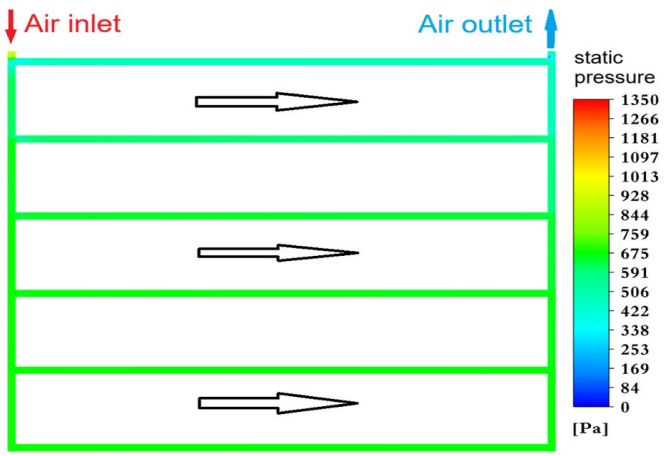


**Figure 18.** Static pressure contours on the longitudinal plane aligned with the pipe axis for the six-pipe EAHE at an inlet airflow velocity of 15 m/s

Figure 19 shows the airflow share in each parallel pipe. The flow fraction decreases from Pipe 1 (25.1%) to Pipe 6 (9.3%), indicating progressive redistribution across branches rather than concentration in a single pipe. The higher share in the first pipes is likely associated with higher available driving pressure near the inlet manifold, while the progressive decline is consistent with the pressure gradient along the manifold as flow is successively extracted by downstream branches. Overall, airflow is distributed across all pipes, with upstream branches carrying a larger share, consistent with the static-pressure field shown in Figure 18.

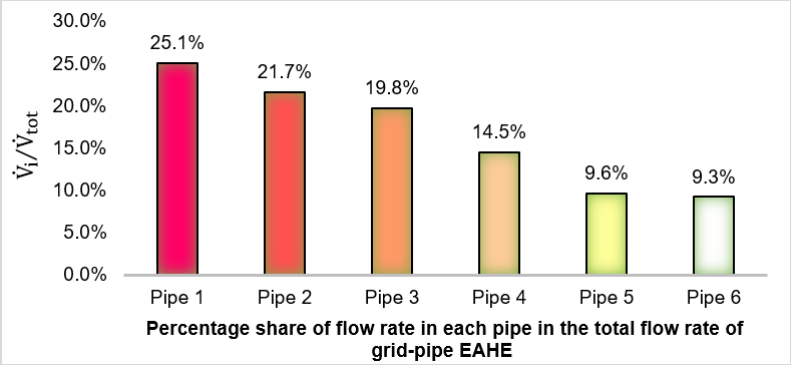


**Figure 19.** Airflow shares in each parallel pipe for the U-type EAHE at an inlet airflow velocity of 15 m/s

These diagnostics suggest that refining the manifold design (e.g., manifold diameter, branch length, and number of branches) is an effective lever to improve flow uniformity and reduce $\Delta P$.

### 3.5 Scalability and Engineering Constraints

This work demonstrates EAHE performance at pilot scale using a buried multi-pipe configuration (total buried length and depth as reported in Section 2). Scaling to larger agricultural greenhouses is feasible but remains design specific. Increasing pipe length (i.e., heat-transfer area) can improve thermal performance, but it typically increases pressure drop and fan-energy demand, requiring an explicit thermal–hydraulic trade-off. In multi-pipe systems, manifold design and overall geometry also influence airflow distribution uniformity and total pressure losses and should therefore be considered during scale-up.

Practical constraints include excavation area and burial depth, pipe spacing, maintenance access, and available electrical power for fans. Accordingly, the present results should be interpreted as a validated pilot-scale reference and a basis for engineering sizing, rather than a universal guarantee for all agricultural deployments.

### 3.6 Indicative Baseline Comparison

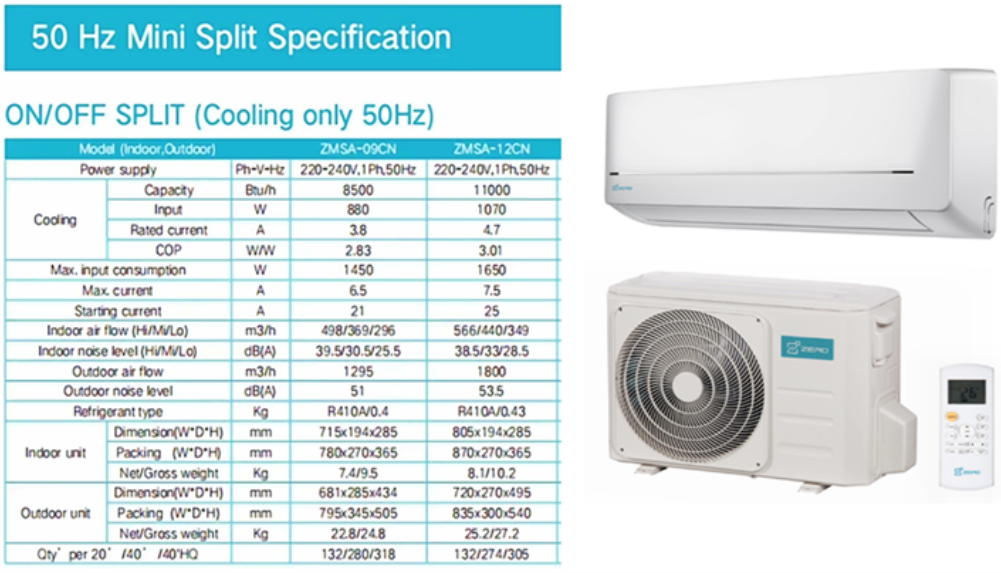

50 Hz Mini Split Specification

ON/OFF SPLIT (Cooling only 50Hz)

| Model (Indoor,Outdoor) | | | ZMSA-09CN | ZMSA-12CN |
|---|---|---|---|---|
| Power supply | | Ph-V-Hz | 220-240V,1Ph,50Hz | 220-240V,1Ph,50Hz |
| Cooling | Capacity | Btu/h | 8500 | 11000 |
| | Input | W | 880 | 1070 |
| | Rated current | A | 3.8 | 4.7 |
| | COP | W/W | 2.83 | 3.01 |
| Max. input consumption | | W | 1450 | 1650 |
| Max. current | | A | 6.5 | 7.5 |
| Starting current | | A | 21 | 25 |
| Indoor air flow (Hi/Mi/Lo) | | m3/h | 498/369/296 | 566/440/349 |
| Indoor noise level (Hi/Mi/Lo) | | dB(A) | 39.5/30.5/25.5 | 38.5/33/28.5 |
| Outdoor air flow | | m3/h | 1295 | 1800 |
| Outdoor noise level | | dB(A) | 51 | 53.5 |
| Refrigerant type | | Kg | R410A/0.4 | R410A/0.43 |
| Indoor unit | Dimension(W*D*H) | mm | 715x194x285 | 805x194x285 |
| | Packing (W*D*H) | mm | 780x270x365 | 870x270x365 |
| | Net/Gross weight | Kg | 7.4/9.5 | 8.1/10.2 |
| Outdoor unit | Dimension(W*D*H) | mm | 681x285x434 | 720x270x495 |
| | Packing (W*D*H) | mm | 795x345x505 | 835x300x540 |
| | Net/Gross weight | Kg | 22.8/24.8 | 25.2/27.2 |
| Qty' per 20' /40' /40'HQ | | | 132/280/318 | 132/274/305 |

**Figure 20.** Manufacturer mini-split specification (50 Hz)

The EAHE provided 2011–2942 W of cooling, while the fan electrical demand was 42–144 W. To contextualize potential energy savings, manufacturer specification sheets for 50 Hz mini-split units in a comparable capacity class (8500–11000 Btu/h $\approx$ 2491–3224 W) were used; this report rated cooling electrical inputs of approximately 880–1070 W (Figure 20). Therefore, for a similar order of cooling duty, the EAHE fan power corresponds to roughly 4%–16% of the electrical input of conventional vapor-compression cooling (indicative baseline). This comparison is provided for context because catalog ratings are reported under standardized conditions, and a direct side-by-side greenhouse test was not performed.

### 3.7 Comparison with Similar EAHE Studies in Hot Climates

To place the present results in context, Table 8 summarizes representative EAHE studies in hot/arid climates and/or greenhouse applications. Because systems differ in geometry, burial depth, soil conditions, and airflow rates, the comparison is indicative rather than a direct benchmark. Nevertheless, the reported ranges help position the temperature depression and electrical demand achieved by the present U-type multi-pipe EAHE within current practice.

**Table 8.** Contextual comparison of EAHE performance in hot/arid climates (selected studies)

| Study | Location/ Climate | Application & Configuration | Burial Depth and Geometry | Key Reported Cooling Indicator (s) |
|---|---|---|---|---|
| Present study | Nasiriyah, Iraq (hot summer) | Greenhouse-coupled EAHE; U-type multipipe grid with inlet/outlet manifolds. | Depth = 3.5 m; 6 parallel PVC pipes (L = 6.93 m each; total L = 53 m); D = 0.1016 m. | Outlet air remained $\sim$ 31–38°C with ambient >50°C; $\Delta T >$ 13°C (July-October); cooling = 2011–2942 W with fan power = 42–144 W. |
| [12] | New Delta, Egypt (arid) | Geothermal assessment for greenhouse applications (EAHE model). | Reference single-pipe PVC EAHE: depth $\approx$ 4 m; L = 50 m; D = 0.1016 m; v $\approx$ 2 m/s. | Subsoil temperature variation $\leq$1.5°C at 4 m depth; indicative single-pipe cooling capacity $\approx$400 W (heating $\approx$ 300 W ). |
| [28] | Biskra, Algeria (hot-arid) | EAHE for building precooling (experimental). | Depth $\approx$ 3 m; single PVC pipe, L $\approx$ 56 m. | Reported maximum cooling reductions up to $\sim$18°C versus ambient during hot daytime hours. |
| [29] | Basra, Iraq (hot) | EAHE for poultry-barn ventilation (experimental); dry vs wetted soil cases. | Depth $\approx$ 2 m (EAHE installed in soil). | During hottest hours, outlet air $\approx$37.35°C (wetted) vs. 38.91°C (dry); wetting improved COP (6.41 vs. 5.07). |

## 4 Conclusions

• The greenhouse-coupled EAHE demonstrated stable pilot-scale pre-cooling performance under the hot climatic conditions of Nasiriyah during July–October 2025.

• The EAHE outlet air temperature remained relatively stable throughout the day, typically ranging between 31 and 34°C, with a moderate rise at midday. These monthly average values (July–October) indicate stable daily performance and reflect the large thermal inertia of the surrounding soil, despite ambient temperatures exceeding 50°C.

• Supplying pre-cooled air moderated the greenhouse air temperature, maintaining it around 34°C for most sunlit hours and rising gradually toward 39°C under peak solar loading.

• Total pressure drops and fan power increased with airflow velocity, indicating a clear thermal–hydraulic trade-off between cooling capacity and energy consumption.

• Among the tested conditions, the highest cooling output with acceptable fan-energy consumption occurred at 15 m/s. The best energy efficiency occurred at lower velocity ($\approx$13 m/s) under moderate loads, indicating that the optimal operating velocity depends on cooling demand.

• Thermal effectiveness remained high under all tested conditions (68%–75%), and the monthly cooling potential ($\Delta T$) exceeded 13°C during July–October. This indicates strong soil–air thermal interaction during the cooling season and supports the observed stability of the EAHE under local hot-climate conditions.

• CFD–experiment validation showed consistent velocity trends, with deviations of 8%–9.3% for $T_o$ and 8.6%–13.7% for $\Delta P$. CFD results at vi =15 m/s indicated a gradual pressure decrease along the manifold and a non-uniform but smoothly varying branch flow allocation, with upstream branches carrying a larger share. These

diagnostics help interpret the measured $\Delta P$ and fan-power response and highlight the manifold/branch configuration as an important design factor.

Overall, the EAHE–greenhouse system offers an energy-efficient pilot-scale option for greenhouse air pre-cooling in hot climates and can improve the greenhouse microclimate. Full-scale agricultural deployment is site specific and should be sized based on ventilation demand, soil conditions, and available installation area. Design should explicitly account for the thermal–hydraulic trade-off between cooling gains and pressure losses (and associated fan power), as well as potential manifold refinements to improve flow distribution.

### Author Contributions

Conceptualization, H.L.T. and M.I.H.; methodology, H.L.T. and M.I.H.; validation, H.L.T. and M.I.H.; formal analysis, H.L.T.; investigation, H.L.T.; resources, H.L.T. and M.I.H.; data curation, H.L.T.; writing—original draft preparation, H.L.T.; writing—review and editing, M.I.H.; visualization, H.L.T.; supervision, M.I.H.; project administration, M.I.H. All authors were actively involved in discussing the findings and refining the final manuscript.

### Data Availability

The data used to support the findings of this study are available from the corresponding author upon request.

### Conflicts of Interest

The authors declare that they have no conflicts of interest.

### References


[1] Ł. Amanowicz and J. Wojtkowiak, "An effect of flow nonuniformity in earth-to-air multi-pipe heat exchangers (EAHEs) on their thermal performance," in *Proceeding XIII International Conference Air & Heat–Water & Energy*, Wrocław–Kudowa, Poland, 2011. https://doi.org/10.15199/9.2017.12.3

[2] Ł. Amanowicz and J. Wojtkowiak, "Experimental investigation and CFD simulation of multi-pipe earth-to-air heat exchangers (EAHEs) flow performance," *E3S Web Conf.*, vol. 22, p. 2, 2017. https://doi.org/10.1051/e3sconf/20172200002

[3] Ł. Amanowicz and J. Wojtkowiak, "Validation of CFD model for simulation of multi-pipe earth-to-air heat exchangers (EAHEs) flow performance," *Therm. Sci. Eng. Prog.*, vol. 5, pp. 44–49, 2018. https://doi.org/10.1016/j.tsep.2017.10.018

[4] Ł. Amanowicz, "Influence of geometrical parameters on the flow characteristics of multi-pipe earth-to-air heat exchangers–experimental and CFD investigations," *Appl. Energy*, vol. 226, pp. 849–861, 2018. https://doi.org/10.1016/j.apenergy.2018.05.096

[5] S. F. Ahmed, M. T. O. Amanullah, M. M. K. Khan, M. G. Rasul, and N. M. S. Hassan, "Parametric study on thermal performance of horizontal earth pipe cooling system in summer," *Energy Convers. Manag.*, vol. 114, pp. 324–337, 2016. https://doi.org/10.1016/j.enconman.2016.01.061

[6] N. Sakhri, Y. Menni, A. J. Chamkha, G. Lorenzini, H. Ameur, N. Kaid, and M. Bensafi, "Experimental study of an earth-to-air heat exchanger coupled to the solar chimney for heating and cooling applications in arid regions," *J. Therm. Anal. Calorim.*, vol. 145, no. 6, pp. 3349–3358, 2021. https://doi.org/10.1007/s10973-020-09867-6

[7] S. N. Ahmad and O. Prakash, "Thermal performance of earth–air heat exchanger using an experimental test rig," *Arab. J. Sci. Eng.*, vol. 48, pp. 11 665–11 678, 2023. https://doi.org/10.1007/s13369-022-07532-8

[8] M. I. Hasan and S. W. Noori, "Numerical investigation of earth to air heat exchanger for cooling and heating applications," in *Proceeding 3rd International Scientific Conference*, Basra, Iraq, 2018, pp. 1–10.

[9] M. I. Hasan and S. W. Noori, "A study of the potential of using the earth to air heat exchanger for cooling and heating of residential buildings in Iraq," *Heat Transfer–Asian Res.*, vol. 48, no. 8, pp. 3902–3927, 2019. https://doi.org/10.1002/htj.21574

[10] M. H. Ali, Z. Kurjak, and J. Beke, "Investigation of earth air heat exchangers functioning in arid locations using MATLAB/Simulink," *Renew. Energy*, vol. 209, pp. 632–643, 2023. https://doi.org/10.1016/j.renene.2023.04.042

[11] E. Hummood, M. I. Hasan, and G. Abd, "Investigating the effects of disturbed soil thickness on the performance of earth–air heat exchanger," *Int. J. Heat Technol.*, vol. 42, no. 3, pp. 1101–1110, 2024. https://doi.org/10.18280/ijht.420337

[12] A. Hegazy and S. Z. Mohamed, "Unlocking geothermal energy for sustainable greenhouse farming in arid regions: A remote-sensed assessment in Egypt's new delta," *Sci. Rep.*, vol. 13, no. 1, 2023. https://doi.org/10.1038/s41598-023-48667-4

[13] N. Sakhri, A. Kifouche, A. Kaddour, N. Chenini, S. Larguech, G. Chambashi, and Y. Menni, "Thermal and economic performance of an earth–air heat exchanger system for indoor climate control in arid winter environments," *Int. J. Low-Carbon Technol.*, vol. 20, pp. 855–864, 2025. https://doi.org/10.1093/ijlct/ctaf046

[14] A. Nauta, S. H. Tasnim, and W. D. Lubitz, "Simulation of an earth-air heat exchanger in a commercial greenhouse to improve energy efficiency," *J. Biosyst. Eng.*, vol. 48, pp. 291–308, 2023. https://doi.org/10.1007/s42853-023-00188-8

[15] S. E. Sofyan, T. M. I. Riayatsyah, E. Hu, A. Tamlicha, T. M. R. Pahlefi, and H. B. Aditiya, "Computational fluid dynamic simulation of earth air heat exchanger: A thermal performance comparison between series and parallel arrangements," *Results Eng.*, vol. 24, p. 102932, 2024. https://doi.org/10.1016/j.rineng.2024.102932

[16] M. I. Hasan and S. W. Noori, "Evaluating the influence of some design and environmental parameters on the performance of earth to air heat exchanger," *J. Eng. Sustain. Dev.*, vol. 22, no. 2, pp. 10–29, 2018. https://doi.org/10.31272/jeasd.2018.2.2

[17] G. Gan, "Simulation of dynamic interactions of the earth–air heat exchanger with soil and atmosphere for preheating of ventilation air," *Appl. Energy*, vol. 158, pp. 118–132, 2015. https://doi.org/10.1016/j.apenergy.2015.08.081

[18] M. Kaushal, "Performance analysis of clean energy using geothermal earth to air heat exchanger (GEAHE) in lower himalayan region–case study scenario," *Energy Build.*, vol. 248, p. 111166, 2021. https://doi.org/10.1016/j.enbuild.2021.111166

[19] M. I. Hasan, S. W. Noori, and A. J. Shkarah, "Parametric study on the performance of the earth-to-air heat exchanger for cooling and heating applications," *Heat Transfer*, vol. 49, no. 4, pp. 1883–1903, 2019. https://doi.org/10.1002/htj.21458

[20] M. I. Hasan and E. K. Jabbar, "Fabricating and testing of the ground coupled air conditioner for residential applications in Iraqi weather," *Energy*, vol. 216, p. 119256, 2020. https://doi.org/10.1016/j.energy.2020.119256

[21] A. Mathur, A. K. Surana, and S. Mathur, "Numerical investigation of the performance and soil temperature recovery of an EATHE system under intermittent operations," *Renew. Energy*, vol. 95, pp. 510–521, 2016. https://doi.org/10.1016/j.renene.2016.04.037

[22] F. X. Niu, Y. Yu, D. Yu, and H. Li, "Heat and mass transfer performance analysis and cooling capacity prediction of earth to air heat exchanger," *Appl. Energy*, vol. 137, pp. 211–221, 2014. https://doi.org/10.1016/j.apenergy.2014.10.008

[23] American Society of Heating, Refrigerating, and Air Conditioning Engineers, *Ashrae Guideline 14-2014: Measurement of Energy, Demand and Water Savings*. American Society of Heating, Refrigerating, and Air Conditioning Engineers, 2014.

[24] C. H. Diedrich, G. H. dos Santos, G. C. Carraro, V. V. Dimbarre, and T. A. Alves, "Numerical and experimental analysis of an earth–air heat exchanger," *Atmosphere*, vol. 14, p. 1113, 2023. https://doi.org/10.3390/atmos14071113

[25] Y. Belloufi, A. Brima, S. Zerouali, R. Atmani, F. Aissaoui, A. Rouag, and N. Moummi, "Numerical and experimental investigation on the transient behavior of an earth air heat exchanger in continuous operation mode," *Int. J. Heat Technol.*, vol. 35, no. 2, pp. 279–288, 2017. https://doi.org/10.18280/ijht.350208

[26] E. de la Rocha Camba and F. Petrakopoulou, "Earth-cooling air tunnels for thermal power plants: Initial design by CFD modelling," *Energies*, vol. 13, p. 797, 2020. https://doi.org/10.3390/en13040797

[27] A. Hegazy, M. Farid, A. Subiantoro, and S. Norris, "Sustainable cooling strategies to minimize water consumption in a greenhouse in a hot arid region," *Agric. Water Manag.*, vol. 274, p. 107960, 2022. https://doi.org/10.1016/j.agwat.2022.107960

[28] O. Hamdi, A. Brima, N. Moummi, and H. Nebbar, "Experimental study of the performance of an earth to air heat exchanger located in arid zone during the summer period," *Int. J. Heat Technol.*, vol. 36, no. 4, pp. 1323–1329, 2018. https://doi.org/10.18280/ijht.360422

[29] W. Morshed, L. Leso, L. Conti, G. Rossi, S. Simonini, and M. Barbari, "Cooling performance of earth-to-air heat exchangers applied to a poultry barn in semi-desert areas of south Iraq," *Int. J. Agric. Biol. Eng.*, vol. 11, no. 3, pp. 47–53, 2018. https://doi.org/10.25165/j.ijabe.20181103.3047

**Nomenclature**

| | |
|---|---|
| CFD | Computational Fluid Dynamics |
| $C_P$ | Specific heat (J·kg$^{-1}$·K$^{-1}$) |
| d | Inner diameter of the pipe (m) |
| EAHE | Earth to Air Heat Exchanger |
| $g$ | Body force (gravity) (m·s$^{-2}$) |
| $k$ | Air thermal conductivity (W·m$^{-1}$·K$^{-1}$) |
| $\dot{m}$ | Mass flow rate (kg·s$^{-1}$) |
| P.P | Pumping power (W) |
| $\boldsymbol{p}$ | Pressure (Pa) |
| PVC | Polyvinyl chloride |
| $Q$ | Heat transfer rate (W) |
| $r$ | Radial coordinate (m) |
| T | Temperature (K), ($^\circ$C) |
| $\boldsymbol{u}$ | Uncertainty |
| $v$ | Velocity (m/s) |
| $\nu$ | Kinematic viscosity ($\mu/\rho$) (m$^2$/s) |
| $\dot{V}$ | Volumetric flow rate (m$^3$·h$^{-1}$) |
| Z | Axial coordinate (m) |
| $\boldsymbol{\Delta P}_{tot}$ | Total pressure losses (Pa) |
| $\varepsilon$ | Effectiveness |
| $\eta^*$ | Overall performance coefficient |
| $\mu$ | Dynamic viscosity (m$^2$·s$^{-1}$) |
| $\boldsymbol{\Phi}$ | Viscous dissipation (W·m$^{-3}$) |
| $\rho$ | Density (kg·m$^{-3}$) |
| $\theta$ | Angular coordinate (rad) |
| i | Inlet |
| o | Outlet |
| s | Undisturbed soil |